

## Terahertz phase microscopy in the sub-wavelength regime

Minwoo Yi, Kanghee Lee, Jin-Dong Song, and Jaewook Ahn

Citation: *Appl. Phys. Lett.* **100**, 161110 (2012); doi: 10.1063/1.4705294

View online: <http://dx.doi.org/10.1063/1.4705294>

View Table of Contents: <http://apl.aip.org/resource/1/APPLAB/v100/i16>

Published by the [American Institute of Physics](#).

---

### Related Articles

The consequences of high injected carrier densities on carrier localization and efficiency droop in InGaN/GaN quantum well structures

*J. Appl. Phys.* **111**, 083512 (2012)

Critical dimensions of highly lattice mismatched semiconductor nanowires grown in strain-releasing configurations

*Appl. Phys. Lett.* **100**, 163108 (2012)

Structural properties of InN films grown on O-face ZnO(000) by plasma-assisted molecular beam epitaxy

*Appl. Phys. Lett.* **100**, 152105 (2012)

Spontaneous emission control of single quantum dots in bottom-up nanowire waveguides

*Appl. Phys. Lett.* **100**, 121106 (2012)

Europium location in the AlN: Eu green phosphor prepared by a gas-reduction-nitridation route

*J. Appl. Phys.* **111**, 053534 (2012)

---

### Additional information on *Appl. Phys. Lett.*

Journal Homepage: <http://apl.aip.org/>

Journal Information: [http://apl.aip.org/about/about\\_the\\_journal](http://apl.aip.org/about/about_the_journal)

Top downloads: [http://apl.aip.org/features/most\\_downloaded](http://apl.aip.org/features/most_downloaded)

Information for Authors: <http://apl.aip.org/authors>

## ADVERTISEMENT

INSTRUMENTS FOR ADVANCED SCIENCE			
	<b>Gas Analysis</b> dynamic measurement of reaction gas streams catalysis and thermal analysis molecular beam studies dissolved species probes fermentation, environmental and ecological studies	<b>Surface Science</b> UHV TPD SIMS end point detection in ion beam etch elemental imaging - surface mapping	<b>Plasma Diagnostics</b> plasma source characterisation etch and deposition process reaction kinetic studies analysis of neutral and radical species
	<b>Vacuum Analysis</b> partial pressure measurement and control of process gases reactive sputter process control vacuum diagnostics vacuum coating process monitoring		
contact Hiden Analytical for further details: <a href="mailto:info@hiden.co.uk">info@hiden.co.uk</a> <a href="http://www.HidenAnalytical.com">www.HidenAnalytical.com</a> CLICK TO VIEW OUR PRODUCT CATALOGUE			

## Terahertz phase microscopy in the sub-wavelength regime

Minwoo Yi,<sup>1</sup> Kanghee Lee,<sup>1</sup> Jin-Dong Song,<sup>2</sup> and Jaewook Ahn<sup>1,a)</sup>

<sup>1</sup>Department of Physics, KAIST, Daejeon 305-701, Korea

<sup>2</sup>Nano Photonics Research Center, Korea Institute of Science and Technology, Seoul 136-791, Korea

(Received 17 February 2012; accepted 5 April 2012; published online 20 April 2012)

Gouy phase shift is a well-known behavior that occurs when a propagating light is focused, but its behavior in the sub-wavelength confinement is not yet known. Here, we report the theoretical and experimental study of the aperture-size dependency of the Gouy phase shift in the sub-wavelength diffraction regime. In experiments carried out with laser-induced terahertz (THz) wave emission from various semiconductor apertures, we demonstrate the use of Gouy phase shift for sub-wavelength THz microscopy. © 2012 American Institute of Physics. [<http://dx.doi.org/10.1063/1.4705294>]

Technological advancement involved in terahertz (THz) frequency wave has attracted a great deal of interest in many different research areas of electromagnetic wave applications, such as material characterization, remote sensing, and biomedical imaging, to list a few.<sup>1,2</sup> For example, THz imaging systems based on THz time-domain spectroscopy (THz-TDS) use either temporally or spectrally resolvable sample information obtained from transmissive or reflective THz signal. However, compared to the plentiful information of a broad-band THz pulse itself gained as a result of spectro-temporal response to a specific material the information used in conventional THz imaging methodologies is rather limited. Recently there have been attempts to use alternative information of THz pulses,<sup>3-6</sup> and there are continuing efforts to discover unconventional usages of THz waves for more advanced and practical measurements for various imaging applications in THz frequency range.

Phase microscope techniques are widely used for a specimen difficult to recognize in an ordinary light microscope.<sup>7-9</sup> Quantitative phase microscopy, in particular, utilizes mathematically derived phase information of optical waves that are transmitted through transparent and colorless objects to visualize the phase profile of the sample.<sup>8,9</sup> In an ordinary THz phase microscope, also known as THz time-of-flight microscopy, the time-delay difference of THz pulses is in correspondence with effective optical path length difference, and, therefore, the spatial phase information  $\phi(x, y)$  that is quantified from a time-delay measurement  $\Delta t(x, y)$  of THz pulses, as

$$\Delta t(x, y) = \frac{\Delta\phi(x, y)}{2\pi f}, \quad (1)$$

where  $f$  is the carrier frequency, which could give the additional information to an ordinary THz amplitude image.<sup>10</sup>

In this letter, we report an observation of geometrically induced phase shift of THz waves and its application to THz imaging of sub-wavelength-scale objects. In an experiment of THz wave generation from semiconducting InAs structure, we found that the pulses radiated from emitters of sub-wavelength scale are temporally shifted compared to the ones from large emitters. With an imaging demonstration, we show that this size-dependent phase shift of diffracted

THz waves can be used as a sensitive means to the recognition of sub-wavelength size structures.

In order to investigate the size-dependent phase shift of THz waves from sub-wavelength apertures, we first consider the original Gouy phase shift, which is size-independent, formulated in the work done by Feng and Winful.<sup>11</sup> The Gouy phase shift is originated from transverse spatial restriction of the wave and the uncertainty principle leads to the reduction of the longitudinal component of a propagation constant  $k$ . So, for a monochromatic wave propagating along  $z$  direction, the effective propagation constant  $\bar{k}_z$  is given by

$$\bar{k}_z = k - \frac{1}{k} \iint (k_x^2 + k_y^2) |F(k_x, k_y)|^2 dk_x dk_y, \quad (2)$$

where  $k_x$  and  $k_y$  are the transverse spatial frequencies, or the vector components of the propagation constant  $k$ , (i.e.,  $k_x^2 + k_y^2 = k^2 - k_z^2$ ), and their distribution  $F(k_x, k_y)$  is the Fourier transform of the spatial profile of the wave. Then, the Gouy phase shift  $\phi_G^o$  is given by

$$\phi_G^o = \int (\bar{k}_z - k) dz. \quad (3)$$

For a Gaussian beam propagation from  $-\infty$  to  $\infty$ , a constant Gouy phase shift  $\phi_G^o = \pi$  is obtained, regardless of the size of the beam.

Now we suppose a situation when the spatial restriction is severe enough that a sub-wavelength size effect should be explicitly considered. If the transverse size of a beam is smaller than the wavelength, the extent of the spatial-frequency distribution  $F(k_x, k_y)$  reaches outside the area of radius  $k$ . There, the longitudinal component  $k_z$  becomes imaginary, (i.e.,  $k_z = i\sqrt{k_x^2 + k_y^2 - k^2}$ ), and an evanescent wave is formed. So, in Eq. (2), the area of integration outside  $k_x^2 + k_y^2 \leq k^2$  needs to be excluded from the calculation. Therefore, the effective propagation constant  $\bar{k}_z$  (real part only) becomes

$$\bar{k}_z = k - k \iint_{k_x^2 + k_y^2 > k^2} |F(k_x, k_y)|^2 dk_x dk_y - \frac{1}{k} \iint_{k_x^2 + k_y^2 < k^2} (k_x^2 + k_y^2) |F(k_x, k_y)|^2 dk_x dk_y, \quad (4)$$

<sup>a)</sup>Electronic mail: jwahn@kaist.ac.kr.

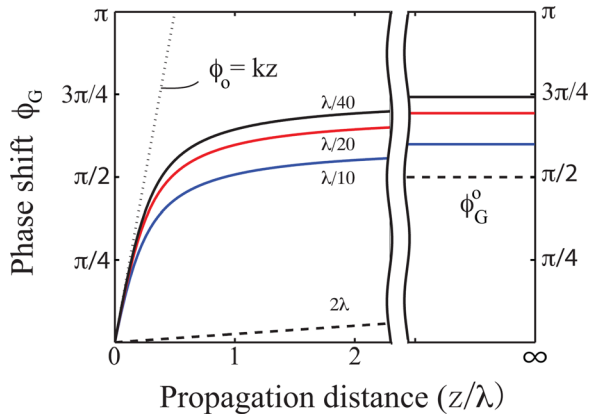


FIG. 1. Calculated Gouy phase shifts  $\phi_G$  of THz pulses radiated from sub-wavelength emission apertures. The Gouy phase shifts  $\phi_G$  for three different-size apertures,  $w_1 = \lambda/40$  (black),  $w_2 = \lambda/20$  (red), and  $w_3 = \lambda/10$  (blue) are plotted with  $\phi_G^o$  (dashed line) of the one from a large-size aperture ( $w = 2\lambda$ ).

where the last two terms contribute to the Gouy phase shift. The given integral calculations are strongly influenced by the relative size of the propagation constant  $k$  compared to the inverse of the transverse spatial extent of the wave. For a beam of sub-wavelength waist  $w$ , it is straightforward to show that Eq. (4) leads to

$$\frac{d\phi_G}{dz} = -k \left( 1 - \frac{w^2 k^2}{4} \right), \quad (5)$$

which is valid for  $w^2 k^2 / 2 \ll 1$ .

Figure 1 summarizes the numerically calculated Gouy phase shifts  $\phi_G$  of THz pulses from sub-wavelength emission apertures of various sizes. Compared to  $\phi_G^o$  (dashed line in the bottom) of the one from a large-size aperture ( $w = 2\lambda$ ), the Gouy phase shifts  $\phi_G$  for three different-size apertures,  $w_1 = \lambda/40$  (black),  $w_2 = \lambda/20$  (red), and  $w_3 = \lambda/10$  (blue), are shown in Fig. 1(d), from the top to the bottom, where the wavelength  $\lambda$  is assumed as  $\lambda = 600$  nm for the rest of the calculation.

The THz waves under consideration are radiated from sub-wavelength-size small emitters of various beam waist  $w_o$ 's located at  $z=0$ , and we are interested in obtaining the  $w_o$ -dependence of the phase shift ( $\phi_G$ ) of the THz pulse, measured at  $z = \infty$ , with respect to the phase of THz pulses from a large-size emitter. Using the chain rule of differentiation, we get

$$\frac{\delta\phi_G}{\delta w_o} = \frac{\partial}{\partial w_o} \int_{w_o}^{\infty} \frac{d\phi_G/dz}{dw/dz} dw = \frac{k}{\alpha}, \quad (6)$$

where  $w$  is the beam waist given as a function of  $z$  and its derivative becomes asymptotically a constant  $\alpha$  before a sub-wavelength propagation (i.e.,  $z \ll \lambda$ ). It is noted that the sub-wavelength wave propagation accumulates negligible phase shift, and, as a result, the size-dependent Gouy phase shift is expected to be linear to the initial beam waist  $w_o$ , at the sub-wavelength aperture limit.

For an experimental verification of the size-dependent phase shift of THz waves, we constructed a laser-THz emission microscope (LTEM) (Ref. 12) as shown in Fig. 2(a). Femtosecond optical laser pulses were used to generate THz pulses via the photo-Dember effect transmissively from a low-bandgap InAs film.<sup>13</sup> The InAs thin film of 1- $\mu\text{m}$  thickness was grown by molecular beam epitaxy on an AlAsSb buffered GaAs substrate. The thickness was optimized by considering effective Dember charge separation and absorption and resolution of THz pulses.<sup>14</sup> The as-grown InAs sample was glued to a sapphire substrate and the substrate and buffer layer were then eliminated by lapping and chemical etching by phosphoric acid solution ( $\text{H}_3\text{PO}_4:\text{H}_2\text{O}_2:\text{H}_2\text{O} = 1:8:80$ , 1.3  $\mu\text{m}/\text{min}$ ). The THz pulses radiated from the InAs thin film were detected by a conventional photo-conductive antenna (PCA) in conventional 4-f imaging geometry.<sup>15</sup> Figure 2(b) shows the schematic THz emission geometry. For a variation of the diameter of excitation area, we have patterned a metal screen with circular holes of various sizes on the surface of InAs. The aperture is formed in a 150-nm-thick gold screen with 15-nm-thick Cr adhesion on the InAs surface by photo-lithographic methods.

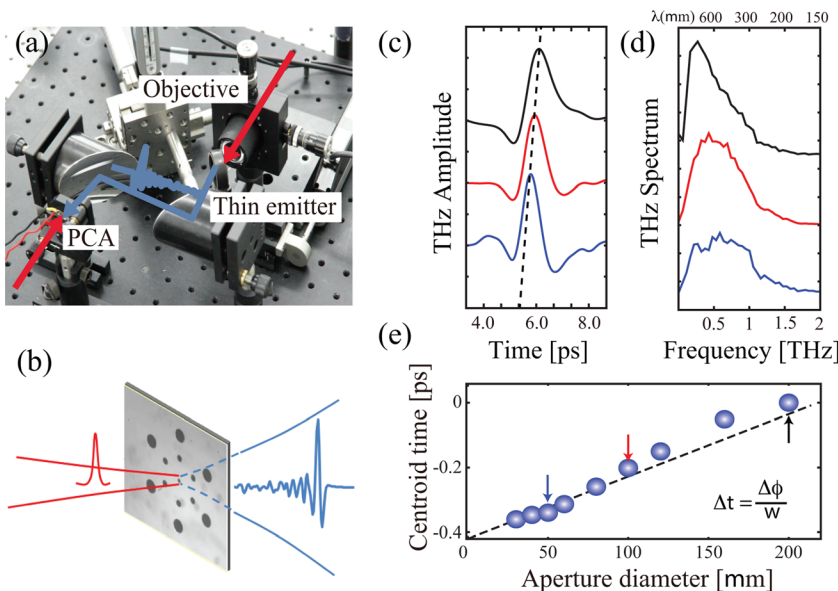


FIG. 2. (a) Layout and (b) schematic diagram of the transmissive sub-wavelength THz phase microscope. (c) Radiated THz pulses and (d) their amplitude spectra for InAs emission apertures of three different sizes; 200 (black), 100 (red), and 50  $\mu\text{m}$  (blue) from top to bottom. (e) The centroid time of radiated THz pulses measured with various size InAs emission apertures from 30 to 200  $\mu\text{m}$  (circle), and the calculated temporal advancement of THz pulses (dashed line).

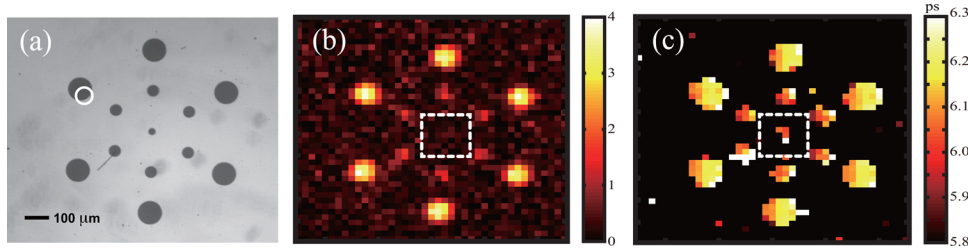


FIG. 3. (a) The microscope image of hexagram which consists of 30-, 50-, and 100- $\mu\text{m}$  diameter InAs emission apertures. (b) Measured THz intensity image and (c) THz temporal phase image with 60- $\mu\text{m}$ -diameter near-infrared pulses.

Typical experimental results are shown in Figs. 2(c) and 2(d), which respectively plot the measured electric field and its Fourier spectra for the THz waves radiated from three different emission apertures. From top to bottom, the smaller aperture is used, the more temporal advancement is observed, as expected.

For a more quantitative analysis of the time-delay measurement, we used the first temporal moment, or the centroid time, defined as

$$\tau(x, y) = \frac{1}{I(x, y)} \int' (t(x, y) - t_0) E^2(x, y; t) dt, \quad (7)$$

where the summation ( $\int'$ ) is taken for positive temporal signal only, (i.e.,  $E(x, y; t) > 0$ ), over a finite time window, and  $t_0$  is the reference time. The energy normalization is also given similarly as  $I(x, y) = \int' E^2(x, y; t) dt$ . Figure 2(e) shows the centroid time of the radiated THz pulses is given as a function of the diameter of the InAs emission aperture. The diameter was varied from 30 to 200  $\mu\text{m}$  and the excitation fluorescence of femtosecond laser pulses was kept constant. As shown in Fig. 2(e), there is a drastic change of the negative time delay as a function of the diameter of the excitation InAs aperture. The THz pulses are further temporally advanced, shifted in the negative time direction, for smaller excitation apertures. Similar behavior has been reported in THz waveguide experiments through sub-wavelength apertures, but the phenomenological explanation in the context of an anomalous index change in waveguide coupling process has not successfully provided a clear picture for its physical origin.<sup>16,17</sup> In our experiment, this temporal phase shift is explained by the geometrically induced phase shift of radiated THz pulses which is dependent of the size of emission apertures. As mentioned above, the size-dependent Gouy phase shift is expected to be linear to the initial beam waist at the sub-wavelength aperture limit. The geometrically induced phase shift of THz waves can be extended to THz imaging of sub-wavelength-scale objects.

For THz phase microscope imaging, we have patterned and tested a hexagram pattern. Figure 3(a) shows the optical image of the sample. The hexagram consists of three different circular InAs apertures: 30, 50, and 100  $\mu\text{m}$ . All the temporal THz signals were measured for all two-dimensional pixels, scanned with 60- $\mu\text{m}$ -diameter near-infrared pulses. A THz intensity image  $I(x, y)$  of the hexagram is shown in Fig. 3(b). The intensity image is not appropriate to resolve the smallest hole due to weak THz signal in the linear scale representation. However, the temporal phase image resolve sub-wavelength 30- $\mu\text{m}$  patterns by using the contrast of temporal phase difference as shown in Fig. 3(c). As shown in Eq. (6)

and Fig. 2(e), the smaller the emission diameter is used and the earlier the centroid time of the radiated THz pulses occurs. We have experimentally confirmed that temporal phase image resolve sub-wavelength 30- $\mu\text{m}$  patterns by using temporal phase difference due to difference arrival time of THz pulses.

In summary, we have considered terahertz phase microscopy in the sub-wavelength regime. With the laser-THz emission microscopy setup, we have studied temporal characteristics of THz pulses generated from sub-wavelength InAs apertures. It is observed that the temporal phase shift of the THz pulse occurs when the THz-wave emission aperture is of sub-wavelength scale. This temporal phase shift is explained by the beam-waist-dependent Gouy phase shift, of which the physical origin is the sub-wavelength spatial confinement of the propagating wave. In the proof-of-principle demonstration of THz phase imaging, we have verified that the temporal phase difference of THz waves can resolve small objects of sub-wavelength size. This effect of geometrically induced phase shift is a generic wave property in the sub-wavelength regime and, therefore, further studies with other wave sources in various frequency range are warranted.

This research was supported by Basic Science Research and Mid-career Researcher Programs through the National Research Foundation of Korea (NRF) funded by the Ministry of Education, Science and Technology (2009-0090843, 2010-0013899). JDS (KIST) acknowledges the support from KIST institutional program.

<sup>1</sup>Y. S. Lee, *Principles of Terahertz Science and Technology* (Springer, New York, 2009).

<sup>2</sup>W. L. Chan, J. Deibel, and D. M. Mittleman, *Rep. Prog. Phys.* **70**, 1325 (2007).

<sup>3</sup>X.-C. Zhang, *Philos. Trans. R. Soc. London A* **362**, 283 (2004).

<sup>4</sup>K. McClatchey, M. T. Reiten, and R. A. Cheville, *Appl. Phys. Lett.* **79**, 4485 (2001).

<sup>5</sup>K. Lee, K. H. Jin, J. C. Ye, and J. Ahn, *Opt. Lett.* **35**, 508 (2010).

<sup>6</sup>K. Lee and J. Ahn, *Appl. Phys. Lett.* **97**, 241101 (2010).

<sup>7</sup>F. Zernike, *Physica* **1**, 689 (1934).

<sup>8</sup>D. Paganin and K. A. Nugent, *Phys. Rev. Lett.* **80**, 2586 (1998).

<sup>9</sup>E. D. Barone-Nugent, A. Barty, and K. A. Nugent, *J. Microsc.* **206**, 194 (2002).

<sup>10</sup>Y. Wang, Z. Zhao, Z. Chen, L. Zhang, K. Kang, and J. Deng, *Appl. Opt.* **50**, 6452 (2011).

<sup>11</sup>S. Feng and H. G. Winful, *Opt. Lett.* **26**, 485 (2001).

<sup>12</sup>T. Kiwa, M. Tonouchi, M. Yamashita, and K. Kawase, *Opt. Lett.* **28**, 2058 (2003).

<sup>13</sup>M. Yi, K. Lee, J. Lim, Y. Hong, Y.-D. Jho, and J. Ahn, *Opt. Express* **18**, 13693 (2010).

<sup>14</sup>K. Liu, J. Xu, T. Yuan, and X.-C. Zhang, *Phys. Rev. B* **73**, 155330 (2006).

<sup>15</sup>M. van Exter and D. Grischkowsky, *Appl. Phys. Lett.* **56**, 1694 (1990).

<sup>16</sup>K. Wynne and D. A. Jaroszynski, *Opt. Lett.* **24**, 25 (1999).

<sup>17</sup>O. Mitrofanov, M. Lee, J. W. P. Hsu, L. N. Pfeiffer, K. W. West, J. D. Wynn, and J. F. Federici, *Appl. Phys. Lett.* **79**, 907 (2001).